Improvement in the methylene blue adsorption capacity and photocatalytic activity of H_2-reduced rutile-TiO_2 caused by Ni(II)porphyrin preadsorption

Carlos A. Páez[1], Stéphanie D. Lambert[1], Dirk Poelman[2], Jean-Paul Pirard[1], Benoît Heinrichs[1]

[1] Université de Liège, Laboratoire de Génie chimique, Institut de Chimie, B6a, B-4000 Liège, Belgium

[2] Ghent University, Lumilab, Department of Solid State Sciences, Krijgslaan 281-S1, B-9000 Ghent, Belgium

APPLIED CATALYSIS B-ENVIRONMENTAL Volume: **106** Issue: **1-2**

Pages: **220-227** DOI: **10.1016/j.apcatb.2011.05.029** Published: **JUL 21 2011**

Keywords

Reduced TiO_2, rutile, Ni(II)-porphyrin, methylene blue photodegradation, visible irradiation, sol-gel process

Abstract

H_2-reduced rutile-TiO_2 xerogel (Ti-700), obtained *via* the sol-gel process, was found to strongly adsorb the Ni(II)-5,10,15,20-tetrakis(4-carboxyphenyl)-porphyrin (NiTCPP) from a methanolic solution, despite its very low specific surface area ($S_{BET} \approx 2$ m^2 g^{-1}). UV/vis spectroscopy analysis showed that after calcination at 700 °C and reduction under H_2 flow at 400 °C, the TiO_2-xerogel increased its NiTCPP-adsorption capacity by surface area unit by up to 120 times. The effect of the porphyrin presence in the catalytic performances of TiO_2-xerogels was studied through three kinetics models: (i) the pseudo-first-order kinetic model; (ii) the pseudo-second-order kinetic model, which are used both to describe the adsorption rate based on the adsorption capacity of the catalysts; and (iii) the Langmuir-Hinshelwood kinetic model which is used to describe the photocatalytic degradation rate of methylene blue (MB). A significant improvement in the efficiency of Ti-700 was observed after the porphyrin-adsorption process (NiTCPP/Ti-700): MB-adsorption capacity at equilibrium and the apparent MB-photoconversion constant, k_{app}, of NiTCPP/Ti-700 were both up to 2 times higher than those observed for the Ti-700.

1. **Introduction**

Photocatalytic degradation of pollutants on the surface of TiO_2 has been intensively studied as a way to solve environmental problems relating to wastewater and polluted air [1-3]. Anatase and rutile are the most commonly used crystalline structures of TiO_2. Anatase shows a higher photocatalytic activity, which is usually attributed to its higher specific surface area and its favourable band gap energy (E_g) [4]. However, its large band gap ($E_g \cong 3.2$ eV) requires the use of UV light ($\lambda \leq 380$ nm) to inject electrons into the conduction band ($TiO_2(e^-_{CB})$) and to leave holes in the valence band ($TiO_2(h^+_{VB})$) [5]. This limits the use of sunlight or visible light as an irradiation source in photocatalytic reactions on anatase-TiO_2. The lower band gap energy of rutile-TiO_2 ($E_g \cong 3.02$ eV) allows rutile to potentially absorb more solar energy than anatase [6]. However, the anatase-to-rutile phase transition leads to the collapse of the TiO_2 specific surface area [7], resulting in a decrease in photocatalytic activity [1, 8-11]. Low specific surface area and therefore low adsorption capacity lead to strong limitations in exploiting the photocatalytic activity of rutile. However, rutile-TiO_2 has some advantages over anatase-TiO_2 such as a higher refractive index, a higher dielectric constant, a higher electrical resistance and a higher chemical stability [12].

Several studies have recently been performed to enhance the photocatalytic activity of rutile-TiO_2 through modification of its surface *via* thermal or chemical treatment. On the one hand, Mohamed *et al.* [13] obtained a good activity in the photocatalytic degradation of methylene blue (MB) dye under visible light irradiation with rutile-TiO_2 after chemical treatment with NH_4VO_3 and $(NH_4)_2SO_4$. They emphasized that MB degradation may be achieved due to basic sites detected on the modified surface. On the other hand, Páez *et al.* [14] synthesized an H_2-reduced rutile-TiO_2 xerogel of low specific surface area with a better MB-photodegradation capacity than both analogous

anatase-TiO_2 xerogels and commercial Degussa TiO_2-P25. The authors assumed that after thermal treatments, *i.e.* calcination at 700 °C and reduction at 400 °C under hydrogen flow, the high degree of reduction undergone by the rutile-TiO_2 caused a significant number of TiO_2 surface defect sites, increasing the number of active sites for the adsorption of MB. Thus, the MB-photodegradation capacity observed for rutile-TiO_2 xerogel is possibly due to a combined effect of: (i) the sensitivity of rutile to visible light irradiation due to its low band gap and (ii) electron transfer from photoexcited MB adsorbed onto the TiO_2 xerogel surface, similar to the effect observed on the TiO_2-P25 surface sensitized with phthalocyanines [15-17] or Ru(II) complexes [18-20]. Thermal treatment is also used to activate the TiO_2 surface for the chemical adsorption of polypyridil or porphyrin complexes [21-25]. Specifically, metallic-5,10,15,20-tetrakis(4-carboxyphenyl)-porphyrins MTCPP (M= Zn, Fe, Cu and metal-free) on anatase-TiO_2 are used as photosensitizers because of their very strong optical absorption in the visible region (400-450 nm region, Soret band) and high chemical stability, and because of the chemical reactivity of their carboxy-substituent groups used for the adsorption process [26-28]. Therefore, the TiO_2-surface defect sites generated after thermal treatment have oxidation-reduction properties that favour a fast and stable adsorption of oxygen-containing organic molecules [4, 29], such as carboxyphenyl porphyrins. In this context, it is interesting to take advantage of the high degree of reduction undergone by rutile-TiO_2 xerogel after thermal treatment (Ti-700), for the adsorption of well known and chemically stable tetracarboxy-substituted porphyrin photosensitizers.

In this work, the effect of nickel(II)-5,10,15,20-tetrakis(4-carboxyphenyl)-porphyrin adsorption (NiTCPP) on the MB-photodegradation activity of H_2-reduced rutile-TiO_2 xerogel (Ti-700) was studied through the Langmuir-Hinshelwood kinetic model.

Additionally, in order to provide a more complete approach of the catalytic mechanism and to investigate the influence of porphyrin in the MB-absorption capacity of the TiO_2 surface, a complementary study was performed and analyzed through pseudo-first-order and pseudo-second-order kinetic models. These adsorption kinetic models are typically used to study highly absorbent materials, such as activated carbons, carbon nanotubes, silica or alumina, and are rarely proposed to study photocatalysts like TiO_2 and functionalized-TiO_2. In this work, the use of these kinetics models allowed; (i) to observe the effect of the porphyrin during the MB-adsorption process and (ii) to propose a spatial arrangement of the interaction between porphyrin and MB molecules into rutile-TiO_2 surface.

2. **Experimental**

2.1 Synthesis of H_2-reduced TiO_2 xerogel

H_2-reduced rutile-TiO_2 xerogel was prepared from tetraisopropoxy titanium(IV) (TIPT, 98% Janssen Chemical) in methoxyethanol (Sigma-Aldrich, 99.8%) according to a reported procedure [14, 30]. First, 77.34 mL of TIPT was mixed with 206.1 mL of 2-methoxyethanol under a nitrogen atmosphere. Then 10.35 mL of distilled water in 206.1 mL of 2-methoxyethanol was added dropwise. The solution vessel was then tightly closed and heated up to 70 °C for 24 h to perform gelation and ageing, and then dried under vacuum at 150 °C for 24 h. The resulting xerogel was crushed and successively washed with deionized water and methanol. This sample is referred to as Ti-NC.

Ti-NC was calcined at 700 °C under flowing air for 12 h. After calcination, the sample was reduced by heating in pure flowing hydrogen (0.23 mmol s^{-1}) at a rate of 400 °C h^{-1} up to 400 °C. This temperature was maintained for 3 h. The sample that received this calcination/reduction treatment is referred to as Ti-700.

2.2 Synthesis of Ni(II) tetrakis(4-carboxy-phenyl)porphyrin (NiTCPP)

Following the protocol proposed in the literature [26, 31] the synthesis of NiTCPP was performed *via* classical metallation of free-metal tetrakis(4-carboxy-phenyl)porphyrin (TCPP), which was obtained by the well-known method proposed by Longo *et al.* [28, 32]. First, previously dehydrated (110 °C for 12 h) Ni(II) chloride hexahydrate (1.55 g, 0.012 mol) was added to a solution of 0.5 g of the free-metal porphyrin (TCPP, 0.63 mmol) in 50 mL of *N*,*N*-dimethylformamide (DMF), and refluxed for 12 h. Then, the precipitate was dissolved in 0.1 M NaOH solution and reprecipitated by adding 1 M HCl solution. FT-IR: ν (cm^{-1}) 1606 (C=C); 1119, 1508, 1499, 1005 (P ring); 1702 (C=O); 1405, 1273 (O–C–O). ^{1}H NMR (CD_3OD): δ (ppm) 8.83 (s, 8H), 8.43 (d, 8H), 8.31 (s, 8H). UV-vis (CH_3OH): λ (nm) 409 (Soret band), 525 (Q band).

2.3 NiTCPP adsorption

NiTCPP was adsorbed overnight onto the surface of TiO_2 xerogel powder (Ti-NC or Ti-700) from a 0.3 mmol L^{-1} solution of porphyrin in methanol at room temperature and under vigorous stirring. The solid was separated by centrifugation and filtration. The final concentration of NiTCPP in the resultant methanolic solution was analysed by UV/vis spectroscopy at 410 nm. The amount of adsorbed porphyrin was determined from the difference between the initial (0.3 mmol L^{-1}) and final concentrations of NiTCPP in the solution. The amounts of NiTCPP adsorbed were: 7.13 μmol g^{-1} onto Ti-NC and 6.27 μmol g^{-1} onto Ti-700. Finally, the wet powders NiTCPP/Ti-NC and NiTCPP/Ti-700 were successively washed with methanol, washed with distilled water, and dried at 60 °C for 12 h.

2.4 Characterization

The crystalline structure of Ti-700 was determined by XRD with a Siemens D5000 X-ray diffractometer using Cu-Kα radiation. The mean crystallite size, L, was estimated by transmission electron microscopy (TEM, JEOL JEM-4000EX) operated at an accelerating voltage of 400 kV. The texture of the xerogel was examined by nitrogen adsorption-desorption. Isotherms were measured with a Fisons Sorptomatic 1990. These isotherms provide the specific surface area, S_{BET}, and the specific pore volume calculated from the nitrogen adsorbed volume at saturation, V_p [30, 33]. UV/vis spectra of methanolic solutions were obtained on a Genesys 10S UV-vis (Thermo Scientific). UV/vis diffuse reflectance spectra (DR-UV/vis) of the dry powders were performed on a Varian Cary 5000 UV/vis/NIR spectrophotometer, equipped with a Varian External DRA-2500 integrating sphere, using $BaSO_4$ as the reference. The band gap energy of semiconductor material (E_g) was determined in accordance with the literature [14, 30]. FT-IR spectra were recorded with a Bruker IS-88 spectrometer at room temperature in the region of 400-4000 cm^{-1} (resolution 4 cm^{-1}; 16 scans/spectrum). ^1H NMR was performed on Bruker Avance 200 and 400 spectrometers.

2.5 Adsorption kinetic of methylene blue (MB)

Batch adsorption kinetic experiments were carried out by agitating 0.018 g of each catalyst (Ti-NC, NiTCPP/Ti-NC, Ti-700, NiTCPP/Ti-700) in 18 mL of MB aqueous solution (20 μmol L^{-1}) in a glass flask placed in a thermostatic bath at a constant temperature of 22 °C, in the dark. After a given time, the catalyst was removed by centrifugation and the remaining MB concentration in the solution was measured by light absorption of the clear solution at 664 nm, which corresponds to the maximum MB absorption wavelength.

2.6 Photocatalytic activity

The photocatalytic degradation of MB under visible light irradiation ($\lambda \geq 420$ nm), was carried out using a batch reactor with external halogen lamp (150 W, 230 V) powered at 110 V. A circulating water jacket was used to cool the batch reactor and the temperature was kept at around 25 °C. In a typical experiment, the catalyst was added to an aqueous solution (20 μmol L^{-1}) of MB to reach a concentration of 1 g L^{-1}. In all cases, the mixture was kept in the dark for 60 min to ensure that the adsorption-desorption equilibrium was reached before irradiation. After a given irradiation time, the catalyst was removed by centrifugation and the remaining MB concentration in the solution was measured by light absorption of the clear solution at 664 nm.

3. **Results**

3.1 Catalyst characterization

As reported in previous studies [14, 30], calcination at 700 °C leads to well defined diffraction peaks corresponding to the rutile phase with a maximum crystallite size, *L*, of 85 nm, as displayed in Table 1. Table 1 also shows the values of the specific surface area, S_{BET}, and the specific pore volume, V_p. While the uncalcined TiO_2 xerogel sample (Ti-NC) develops a notable porous texture, its calcination at 700 °C induces a significant collapse of its specific surface area from 260 m^2 g^{-1} to around 2 m^2 g^{-1} for Ti-700. This textural collapse is accompanied by a significant change in the chemical TiO_2-surface properties observed from the IR absorbance spectrum (Fig. 1). Besides the fundamental vibrations of TiO_2 observed at around 500 cm^{-1} (ascribed to Ti–O and Ti–O–Ti bonds) [34-36], the vibration modes of Ti^{4+}O-H and the adsorbed H_2O observed in Ti-NC (found at around 3300 and 1630 cm^{-1}, respectively) totally disappear after calcination/reduction treatment in Ti-700. Additionally, bands of approximately 2900 cm^{-1} and in the 900-1500 cm^{-1} region both associated with organic residues also disappear in Ti-700. Finally, the calcination/reduction treatment of Ti-NC also leads to

a dramatic increase in absorbance in the entire IR spectrum, together with the appearance of multiple peaks in the OH stretching region (approximately 3600 cm^{-1}). Both phenomena have been associated to a high degree of reduction in Ti-700 [14].

DR-UV/vis spectra of all samples (Ti-NC, NiTCPP/Ti-NC, Ti-700, NiTCPP/Ti-700) are shown in Fig. 2. In all four samples, which contain TiO_2-xerogel, a maximal absorption band (λ_{max}) is observed in the 310 – 360 nm region. This band corresponds to the $O^{2-}(2p) \rightarrow Ti^{4+}(3d)$ charge transfer process in TiO_2 (anatase: λ_{max}= 325 nm; rutile: λ_{max}= 350 nm) [37]. In addition, two new bands appear in spectra of NiTCPP/Ti-NC and NiTCPP/Ti-700 at around 416 and 528 nm (Fig. 2). Typically, these absorptions are found in metallic-porphyrins and correspond to Soret bands and Q bands, respectively [26]. In the free-NiTCPP sample, these bands are found at 405 and 425 nm (Fig. 2).

The UV/vis spectroscopy analysis (at 410 nm) of the methanolic solutions (before and after the NiTCPP-adsorption process) showed that the amount of NiTCPP adsorbed by the xerogel decreased from 7.13 μmol g^{-1} for Ti-NC to 6.27 μmol g^{-1} for Ti-700. However, the amount of NiTCPP adsorbed by surface area unit increased significantly: from 0.016 molecules nm^{-2} on Ti-NC to 1.88 molecules nm^{-2} on the Ti-700 surface. These values were calculated by dividing the number of NiTCPP-molecules adsorbed (per gram of support) by the specific surface area, S_{BET}, of each TiO_2-xerogel (Table 1).

3.2 Adsorption kinetics of methylene blue

To study the effect of the presence of porphyrin in MB-adsorption kinetics on the Ti-700 and Ti-NC surfaces, two kinetic models were applied: (i) the pseudo-first-order model; and (ii) the pseudo-second-order model. Both models describe the adsorption

rate based on the adsorption capacity of the support. In accordance with Ho [38], the pseudo-first-order model can be written as:

$$\frac{dq_t}{dt} = k_1\left(q_{eq} - q_t\right) \quad (1)$$

where q_{eq} (mol g^{-1}) and q_t (mol g^{-1}) are the adsorption capacities (or the amounts of MB-adsorbed) at equilibrium and at time t (s), respectively and k_1 (s^{-1}) is the constant of the pseudo-first-order kinetic. Integration of Eq. 1, with the integration limits of $t = 0$ to $t = t$ and $q_t = 0$ to $q_t = q_t$, yields:

$$q_t = q_{eq}\left(1 - \exp\left(-k_1 t\right)\right) \quad (2)$$

Alternatively, Ho and McKay [38, 39] proposed that the driving force of the adsorption process is proportional to the available fraction of surface active sites. The kinetic equation rate can then be rewritten as [38]:

$$\frac{dq_t}{dt} = k_2\left(q_{eq} - q_t\right)^2 \quad (3)$$

After variable separation and integration ($t = 0$ to $t = t$ and $q_t = 0$ to $q_t = q_t$), Eq. (3) gives:

$$q_t = \frac{k_2 {q_{eq}}^2 t}{1 + k_2 q_{eq} t} \quad (4)$$

The kinetic experimental data were correlated and fitted to the kinetic models, Eq. 2 and Eq. 3. Fig. 3 compares the behaviour of q_t as a function of t in these models, with the experimental data obtained for Ti-NC, NiTCPP/Ti-NC, Ti-700 and NiTCPP/Ti-700. For all catalysts, the pseudo-second-order model provided the best correlation of the kinetic experimental data. From the pseudo-second-order kinetic model, it can be observed that for the uncalcined sample (Ti-NC), the k_2 and q_{eq} values (Table 2) are not changed significantly by the presence of porphyrin (NiTCPP/Ti-NC), 1.67 μmol g^{-1} for q_{eq} and 340 g mol^{-1} s^{-1} for k_2. Whereas, for Ti-700, the fitted value of the equation constant, k_2 = 1247 g mol^{-1} s^{-1}, is almost two times higher for the system after porphyrin adsorption,

sample NiTCPP/Ti-700, k_2 = 2394 g mol^{-1} s^{-1} (Table 2). Additionally, after porphyrin adsorption onto the Ti-700 surface, the amount of MB adsorbed at equilibrium, q_{eq}, increased from 1.26 to 2.83 μmol g^{-1}, for Ti-700 and NiTCPP/Ti-700, respectively.

3.3 Photocatalytic activity

The activities of the catalysts were evaluated in the photoconversion of MB at room temperature, under visible light irradiation. The control tests confirmed that MB was not degraded (i) in the dark in the presence of catalyst; or (ii) under light irradiation in the absence of catalyst (referred to as black, Fig. 4). The evolution of MB concentration as a function of time is shown in Fig. 4. As shown in Fig. 4, all reactions were allowed to stand in the dark for a period of 60 min, in order to establish adsorption equilibrium. As reported in section, after 60 min in the dark, about 20% of MB was adsorbed onto the Ti-700 surface, whereas around 7% of MB was adsorbed onto other catalysts. After the light was turned on for 120 min, the MB-concentration continued to decrease. During the irradiation period, MB-photodegradation data were analysed using the Langmuir-Hinshelwood kinetic model [13, 40]:

$$r_S = \frac{kKC}{1+KC} \tag{5}$$

where r_S is the specific degradation reaction rate of MB (mol L^{-1} s^{-1}), C the concentration of MB (mol L^{-1}), k the reaction rate constant (s^{-1}) and K the dye adsorption constant. When the concentration (C) is small enough, Eq. (5) can be simplified in an apparent first-order equation:

$$r_S = kKC = k_{app}C \quad \left(= -\frac{dC}{dt}\right) \tag{6}$$

After integration, Eq. 7 is obtained.

$$-\ln\left(\frac{C}{C_0}\right) = k_{app}t \tag{7}$$

where C_0 is the initial concentration (mol L^{-1}) and t the irradiation time (s). In all cases, a satisfactory linearity was obtained by applying Eq. 7 (Fig. 5). Values of the apparent first-order constant, k_{app}, are reported in Table 2. No significant photocatalytic activities were found in the non-calcined samples, Ti-NC and NiTCPP/Ti-NC, which showed k_{app} values of about 2.17 x 10^{-5} s^{-1}. However, a significant increase in k_{app}, was observed after adsorption of Ni(II)-porphyrin onto the Ti-700 surface (Table 2). The sample calcined and reduced without porphyrin (Ti-700) showed an apparent photoconversion constant of 3.3 x 10^{-5} s^{-1}, whereas the TiO_2-xerogel after porphyrin adsorption displayed a constant of 7.2 x 10^{-5} s^{-1} (Table 2).

4. **Discussion**

The changes observed in the physicochemical properties of TiO_2 xerogel after calcination at 700 °C and high temperature reduction at 400 °C under hydrogen flow (Ti-700) are in accordance with results found in the literature [14, 30]: (i) the formation of TiO_2-rutile as a unique crystalline phase; (ii) the growth of the crystalline size, L, to 85 nm (Table 1); (iii) a strong decrease in the specific surface area, S_{BET}, from 260 to about 2 m^2 g^{-1} (Table 1); (iv) a decrease in the band-gap energy, E_g, from 3.61 to 3.04 eV (Table 1); (v) the elimination of a large proportion of the surface groups: H_2O and -OH (Fig. 1); and (vi) an increase in the number of TiO_2-surface defect sites (oxygen vacancies) as a consequence of the high degree of reduction of Ti-700, which can be detected by the increase in the entire IR-background of the sample after thermal treatment (Fig. 1, [14]).

Several reports show that applying thermal treatment to titanium dioxide can lead to structural changes, which are characteristic of diffusion processes associated with the increased mobility of lattice defects and with changes in oxygen vacancies in the TiO_2-

lattice (such as Ti^{3+}). These changes can affect the adsorption processes through the presence of TiO_2 surface defect sites. In fact, a previous study [14] showed that after calcination at 700 °C and hydrogen reduction at 400 °C, the loss in the specific surface area observed in TiO_2-xerogels was compensated by an increase in the number of Ti-700 surface active sites for the adsorption of methylene blue (MB). In a similar way, several studies have also proposed the use of a thermal pretreatment of TiO_2 for the adsorption of dyes, using temperatures of between 400 and 550 °C, for 30 min [21-25]. This thermal treatment is used because the TiO_2-surface defect sites generated have oxidation-reduction properties that favour the adsorption of oxygen-containing organic molecules [4, 29], such as is observed in the adsorption of NiTCPP onto the Ti-NC and Ti-700 surfaces. The UV/vis spectroscopy analysis of the methanolic solutions here showed that, after calcination/reduction treatment, the amount of NiTCPP adsorbed by area unit onto the Ti-NC surface increased by almost 120 times: from 0.016 molecules nm^{-2} for Ti-NC to 1.88 molecules nm^{-2} for Ti-700. In accordance with Cherian and Wamser [24], up to around 0.43 molecules of tetracarboxy-porphyrin would be supported by surface area unit (nm^2) when porphyrin is adsorbed in a flat geometry and around 1.66 molecules by nm^2 would be supported when porphyrin is adsorbed due to the well-packed edgewise stacking molecules. This means that the formation of the porphyrin-layer presumably occurs: (i) on the Ti-NC surface with flat geometry ($0.016 < 0.43$ molecules nm^{-2}); and (ii) on the Ti-700 surface with a well-packed edgewise stacking porphyrin molecules or with a variety of different adsorption modes including multilayers.

In the DR-UV/vis absorption spectra of the Ti-NC and Ti-700 samples (Fig. 2), some changes were observed after the NiTCPP-adsorption process. Two new absorption bands of around 410 nm and 530 nm revealed the presence of tetracarboxy-porphyrin on

the TiO_2-xerogel surfaces. In addition, a bathochromic shift in the Soret and Q bands of free-NiTCPP was found after NiTCPP-adsorption (NiTCPP/Ti-NC and NiTCPP/Ti-700). This small red shift can be attributed to new interaction between porphyrin and the TiO_2-xerogel surface. These interactions may take place *via* delocalized–π* porphyrin electrons in the conduction band of the TiO_2-xerogel [27], where the geometric orientations of adsorbed-porphyrin may play an important role [41].

In order to obtain information regarding the MB-adsorption mechanism on the surface of TiO_2 xerogels, a study of adsorption kinetics of methylene blue was carried out applying two kinetic models: the pseudo-first-order model and the pseudo-second-order model. Significant changes in the MB-adsorption rate of H_2-reduced rutile-TiO_2 xerogel (Ti-700) were observed as a consequence of the presence of NiTCPP on its surface (NiTCPP/Ti-700). On the one hand, the comparison of the experimental kinetic data shows that the adsorption rate of MB onto NiTCPP/Ti-700 was higher than that obtained on other surfaces: Ti-700, Ti-NC and NiTCPP/Ti-NC (Table 2). On the other hand, while the kinetic data for Ti-NC, Ti-700 and NiTCPP/Ti-NC showed a good concordance with both kinetic models, the kinetic data of NiTCPP/Ti-700 showed better agreement with the pseudo-second-order model (Fig. 3a-b). This means that in all catalysts, the kinetic order is two with respect to the number of available active sites (q_{eq} - q_t) for MB adsorption; see Eq. 1 and Eq. 3. Therefore, the rate expression is not only described by the adsorption capacity of the TiO_2 xerogels; other phenomena should also be considered, such as chemical bonding (chemisorption phenomena) between MB and the TiO_2-surface [39]. From parameters obtained through the pseudo-second-order model (q_{eq}, k_2, Table 2), it was observed that the effect of NiTCPP adsorption was more perceptible in Ti-700 than in Ti-NC. The presence of NiTCPP on the Ti-700 surface increased by almost 2 times the adsorption capacity at equilibrium (q_{eq}) and by 1.8 times

the value of the rate constant, k_2. These phenomena may result from a complexation reaction between MB and porphyrin adsorbed onto the Ti-700 surface, similar to the complexation between MB and tetrakis(4-sulfonatophenyl)phorphyrin (TSPP) studied by Hamai and Satou [42]. These authors reported that MB forms complexes with organic anions such as naphtalenesulfonates, 2-anthracenesulfonate and TSPP in aqueous solutions. From reaction 1:

$$MB + TSPP \rightarrow MB\text{-}TSPP \quad (1)$$

it is proposed that the formation of MB-TSPP complex occurs through interaction between the negatively charged sulphonatophenyl moiety of TSPP and MB, which bears a positive charge.

The structure of the MB cation is shown in Figure 6 [43]. MB is a heteroaromatic molecule that contains a sulphur and a nitrogen atom in its aromatic moiety. The aromatic unit is planar and has two dimethylamino groups attached. The whole molecule is conjugated and the π-orbitals are delocalized over the entire molecule (except for the methyl groups). The positive charge is best stabilized by the N of dimethylamino group and S atoms (Figure 6). Hence, the maximal electrostatic interaction is expected when the longest edges of these atoms are in contact with negatively charged surface sites and/or with functional-surface groups of high electronic density, such as the carboxy function in porphyrin. These interactions may be more favoured when tetra-carboxy-porphyrin is adsorbed edgewise than when it is adsorbed flat onto the Ti-700 surface (Figure 6).

A significant improvement in the efficiency of Ti-700 was observed after the porphyrin-adsorption process (NiTCPP/Ti-700): the apparent MB-photoconversion constant, k_{app}, reached a value of up to 2 times greater than that observed for the Ti-700, Ti-NC and

NiTCPP/Ti-NC samples. After photo-generation of active species such as: $TiO_2(e^-_{CB})$, $TiO_2(h^+_{VB})$, $O_2^{\bullet-}$, $HO_2^{\bullet-}$, $OH^\bullet$ (reactions 2-6, [44]) and in agreement with the analysis proposed by Konstantinou *et al.* [44], the photoconversion mechanism of MB with visible-irradiated TiO_2 follows the Langmuir-Hinshelwood model for four possible situations: (i) the reaction takes place between two adsorbed substances; (ii) the reaction occurs between a radical (such as $O_2^{\bullet-}$, $HO_2^{\bullet-}$, $OH^\bullet$, reaction 7) in solution and an adsorbed MB molecule; (iii) the reaction takes place between a radical linked to the surface and an MB molecule in solution; and or (iv) the reaction occurs with both species being in solution.

$$TiO_2 + h\upsilon \rightarrow TiO_2(e^-_{CB}) + TiO_2(h^+_{VB}) \quad (2)$$

$$TiO_2(h^+_{VB}) + H_2O \rightarrow TiO_2 + H^+ + OH^\bullet \quad (3)$$

$$TiO_2(h^+_{VB}) + OH^- \rightarrow TiO_2 + OH^\bullet \quad (4)$$

$$TiO_2(e^-_{CB}) + O_2 \rightarrow TiO_2 + O_2^{\bullet-} \quad (5)$$

$$O_2^{\bullet-} + H^+ \rightarrow HO_2^\bullet \quad (6)$$

$$MB + OH^\bullet \rightarrow \text{degradation products} \quad (7)$$

In all cases, the expression for the rate equation is similar to the one derived from the L-H model. Although it is not possible to find out whether the process takes place on the surface, in the solution or at the interface, it is likely that the adsorption of MB plays an important role in photocatalytic activity. The improvement in MB adsorption capacity shown by NiTCPP/Ti-700 may explain, in part, the improvement in the photocatalytic activity of Ti-700. In addition, the potential of NiTCPP as a photosensitizer may increase electron transfer from photo-excited NiTCPP to the conduction band of Ti-700, enhancing the production of radicals (reactions 8-10, [44]). This electron transfer mechanism is similar to the one observed in the classical photosensitization of TiO_2

through dye-adsorption (dicarboxypolypyridil-Ru(II) or tetracarboxyphenyl-porphyrin dyes), *via* thermal pre-treatment of TiO_2 (reactions 8-10).

$$TSPP + h\upsilon \rightarrow TSPP * \quad (8)$$

$$TSPP * + TiO_2 \rightarrow TSPP^{\bullet+} + TiO_2(e^-_{CB}) \quad (9)$$

$$TiO_2(e^-_{CB}) + O_2 \rightarrow TiO_2 + O_2^{\bullet-} \quad (10)$$

5. **Conclusion**

A high surface coverage of Ni(II) tetrakis(4-carboxy-phenyl)porphyrin (NiTCPP) in TiO_2-xerogel (Ti-NC) was achieved by calcination at 700 °C and high temperature reduction at 400 °C under hydrogen flow. The following changes were observed in the physicochemical properties of the xerogel after calcination/reduction treatment of Ti-NC: the presence of rutile as the crystalline phase, a decrease in the specific surface area (to 2 m^2 g^{-1}), and a diminution in the band-gap energy (to 3.02 eV). Calcination/reduction treatment also caused an increase in the number of TiO_2-surface active sites for the NiTCPP-adsorption, presumably as a consequence of the mobility of lattice defects and changes in oxygen vacancies in the TiO_2-lattice.

Repeatedly, the presence of NiTCPP-molecules in the H_2-reduced rutile-TiO_2 xerogel surface led to a significant enhancement in its MB-adsorption capacity and in its MB-photocatalytic capacity, under visible light irradiation. On the one hand, the kinetic studies of all samples showed that the MB-adsorption process may be mainly governed by chemisorption phenomena. This was demonstrated by the fact that NiTCPP/Ti-700 was found to be the system showing the highest performance, with q_{eq} and k_2 values of up to 2 times higher than those displayed by the other samples (NiTCPP/Ti-NC, Ti-700 and Ti-NC). This result was probably achieved due to the generation of new rutile-TiO_2 surface active sites for MB-adsorption with high electronic density, such as carboxy-porphyrin substituent groups. On the other hand, NiTCPP/Ti-700 also showed the best

MB-photodegradation activity, up to 2 times higher than that of rutile-TiO_2 without porphyrin (Ti-700). This efficiency in the MB-photocatalytic activity of NiTCPP/Ti-700 could be due to a combined effect of the potential photosensitivity of the rutile-TiO_2 band gap, the increase in MB-adsorption capacity and the electron transfer from photo-excited porphyrin to the surface of Ti-700.

Acknowledgements

C.A. Páez and S.D. Lambert are grateful to the Belgian F.R.S.-FNRS for their postdoctoral research and research associate positions, respectively. The authors also thank the Belgian Fonds de la Recherche Fondamentale Collective (F.R.F.C), the Ministère de la Région Wallonne, FWO-Vlaanderen and the Belgian Interuniversity Attraction Pole INANOMAT (IAP-P6/17) for their financial support.

References

[1] M.R. Hoffmann, S.T. Martin, W. Choi, D.W. Bahnemann, Chem. Rev. 95 (1995) 69-96.

[2] A. Hagfeldt, M. Graetzel, Chem. Rev. 95 (1995) 49-68.

[3] M.A. Fox, M.T. Dulay, Chem. Rev. 93 (1993) 341-357.

[4] A.L. Linsebigler, G. Lu, J.T. Yates, Chem. Rev. 95 (1995) 735-758.

[5] C. Kormann, D.W. Bahnemann, M.R. Hoffmann, J. Phys. Chem. 92 (1988) 5196-5201.

[6] R. Zhang, L. Gao, Q. Zhang, Chemosphere 54 (2004) 405-411.

[7] J.C. Yu, J. Yu, L. Zhang, W. Ho, J. Photochem. Photobiol., A 148 (2002) 263-271.

[8] P. Górska, A. Zaleska, E. Kowalska, T. Klimczuk, J.W. Sobczak, E. Skwarek, W. Janusz, J. Hupka, Appl. Catal., B 84 (2008) 440-447.

[9] Q. Xiao, J. Zhang, C. Xiao, Z. Si, X. Tan, Sol. Energy 82 (2008) 706-713.

[10] G. Li, S. Ciston, Z.V. Saponjic, L. Chen, N.M. Dimitrijevic, T. Rajh, K.A. Gray, J. Catal. 253 (2008) 105-110.

[11] H. Zhang, J.F. Banfield, J. Phys. Chem. B 104 (2000) 3481-3487.

[12] K.-J. Kim, K.D. Benkstein, J. van de Lagemaat, A.J. Frank, Chem. Mater. 14 (2002) 1042-1047.

[13] M.M. Mohamed, M.M. Al-Esaimi, J. Mol. Catal. A: Chem. 255 (2006) 53-61.

[14] C.A. Páez, D. Poelman, J.-P. Pirard, B. Heinrichs, Appl. Catal., B 94 (2010) 263-271.

[15] G. Granados O, C.A. Páez M, F. Martínez O, E.A. Páez-Mozo, Catal. Today 107-108 (2005) 589-594.

[16] J. He, G. Benkö, F. Korodi, T. Polívka, R. Lomoth, B. Åkermark, L. Sun, A. Hagfeldt, V. Sundström, J. Am. Chem. Soc. 124 (2002) 4922-4932.

[17] J. He, A. Hagfeldt, S.-E. Lindquist, H. Grennberg, F. Korodi, L. Sun, B. Åkermark, Langmuir 17 (2001) 2743-2747.

[18] Y. Cho, W. Choi, C.-H. Lee, T. Hyeon, H.-I. Lee, Environ. Sci. Technol. 35 (2001) 966-970.

[19] K. Hara, H. Sugihara, L.P. Singh, A. Islam, R. Katoh, M. Yanagida, K. Sayama, S. Murata, H. Arakawa, J. Photochem. Photobiol., A 145 (2001) 117-122.

[20] J.E. Monat, J.H. Rodriguez, J.K. McCusker, J. Phys. Chem. A 106 (2002) 7399-7406.

[21] A. Kay, M. Graetzel, J. Phys. Chem. 97 (1993) 6272-6277.

[22] M. Gratzel, Nature 421 (2003) 586-587.

[23] M. Gratzel, Nature 414 (2001) 338-344.

[24] S. Cherian, C.C. Wamser, J. Phys. Chem. B 104 (2000) 3624-3629.

[25] K.S. Finnie, J.R. Bartlett, J.L. Woolfrey, Langmuir 14 (1998) 2744-2749.

[26] G. Granados-Oliveros, E.A. Páez-Mozo, F.M. Ortega, C. Ferronato, J.-M. Chovelon, Appl. Catal., B 89 (2009) 448-454.

[27] T. Ma, K. Inoue, H. Noma, K. Yao, E. Abe, J. Photochem. Photobiol., A 152 (2002) 207-212.

[28] K. Kalyanasundaram, N. Vlachopoulos, V. Krishnan, A. Monnier, M. Graetzel, J. Phys. Chem. 91 (1987) 2342-2347.

[29] T.L. Thompson, J.T. Yates, Chem. Rev. 106 (2006) 4428-4453.

[30] B. Braconnier, C.A. Páez, S. Lambert, C. Alié, C. Henrist, D. Poelman, J.-P. Pirard, R. Cloots, B. Heinrichs, Microporous Mesoporous Mater. 122 (2009) 247-254.

[31] R.F. Pasternack, L. Francesconi, D. Raff, E. Spiro, Inorg. Chem. 12 (1973) 2606-2611.

[32] F.R. Longo, M.G. Finarelli, J.B. Kim, J. Heterocycl. Chem 6 (1969) 927-931.

[33] A.J. Lecloux, Catalysis: Science and Technology, Springer, Berlin, 1981.

[34] K. Chhor, J.F. Bocquet, C. Pommier, Mater. Chem. Phys. 32 (1992) 249-254.

[35] T. Bezrodna, G. Puchkovska, V. Shymanovska, J. Baran, H. Ratajczak, J. Mol. Struct 700 (2004) 175-181.

[36] A. Larbot, I. Laaziz, J. Marignan, J.F. Quinson, J. Non-Cryst. Solids 147-148 (1992) 157-161.

[37] J. Araña, A.P. Alonso, J.M.D. Rodríguez, G. Colón, J.A. Navío, J.P. Peña, Appl. Catal., B 89 (2009) 204-213.

[38] Y.-S. Ho, J. Hazard. Mater 136 (2006) 681-689.

[39] Y.S. Ho, G. McKay, Water Res. 34 (2000) 735-742.

[40] A. Houas, H. Lachheb, M. Ksibi, E. Elaloui, C. Guillard, J.-M. Herrmann, Appl. Catal., B 31 (2001) 145-157.

[41] W.M. Campbell, A.K. Burrell, D.L. Officer, K.W. Jolley, Coord. Chem. Rev. 248 (2004) 1363-1379.

[42] S. Hamai, H. Satou, Spectrochim. Acta, Part A 57 (2001) 1745-1750.

[43] G. Hahner, A. Marti, N.D. Spencer, W.R. Caseri, J. Chem. Phys. 104 (1996) 7749-7757.

[44] I.K. Konstantinou, T.A. Albanis, Appl. Catal., B 49 (2004) 1-14.

Table 1. Characteristics of the Ti-NC and Ti-700 samples.

Sample	Crystalline phase (TiO_2)	L^a (nm)	$S_{BET}{}^a$ ($m^2\ g^{-1}$)	$V_p{}^a$ ($cm^3\ g^{-1}$)	$E_g{}^{a,b}$ (eV)
Ti-NC	Amorphous	-	260	0.15	3.61
Ti-700	Rutile	85	2	0.03	3.04

[a] L: crystallite size; S_{BET}: specific surface area; V_p: total specific pore volume; E_g: band-gap energy;
[b] The E_g values were determined in accordance with literature [14].

Table 2. Kinetic parameters of the adsorption and photo-degradation of MB.

Sample	Pseudo-first-order model		Pseudo-second-order model		MB Photo-conversion
	q_{eq} (μmol g^{-1})	k_1 (s^{-1})	q_{eq} (μmol g^{-1})	k_2 (g mol^{-1} s^{-1})	k_{app} x 10^5 (s^{-1})
Ti-NC	0.98	0.0011	1.67	340	2.01
NiTCPP/Ti-NC	1.17	0.0007	1.56	406	2.34
Ti-700	1.01	0.0017	1.26	1247	3.33
NiTCPP/Ti-700	2.54	0.0053	2.83	2394	7.16

Figure 1. IR absorbance spectra of Ti-NC and Ti-700 samples.

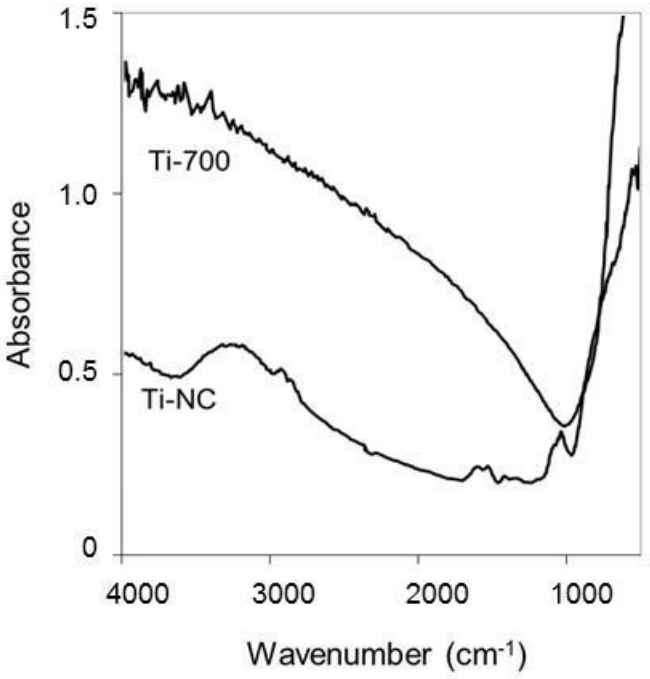

Figure 2. DR-UV/vis spectra of (a) Ti-NC, NiTCPP/Ti-NC, and (b) Ti-700, NiTCPP/Ti-700. For comparison UV/vis spectra of free-NiTCPP is displayed in both spectra.

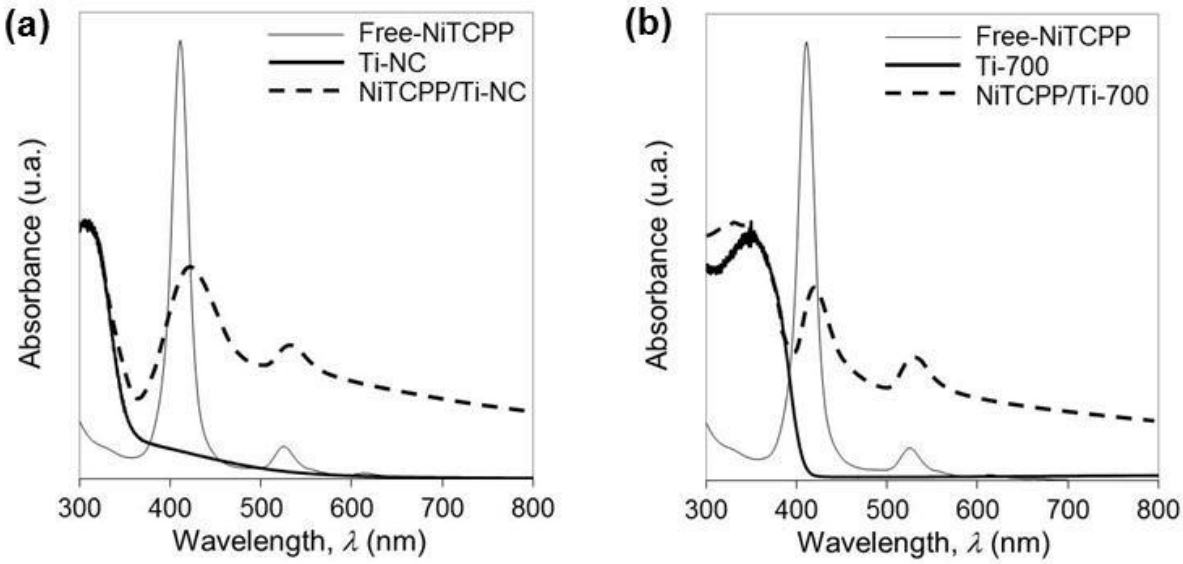

Figure 3. Plot q_t *vs.* *t*; kinetic experimental data of (a) NiTCPP/Ti-NC, Ti-NC and (b) NiTCPP/Ti-700, Ti-700 fitted with pseudo-first-order (- - - -) and pseudo-second-order (——) kinetics models.

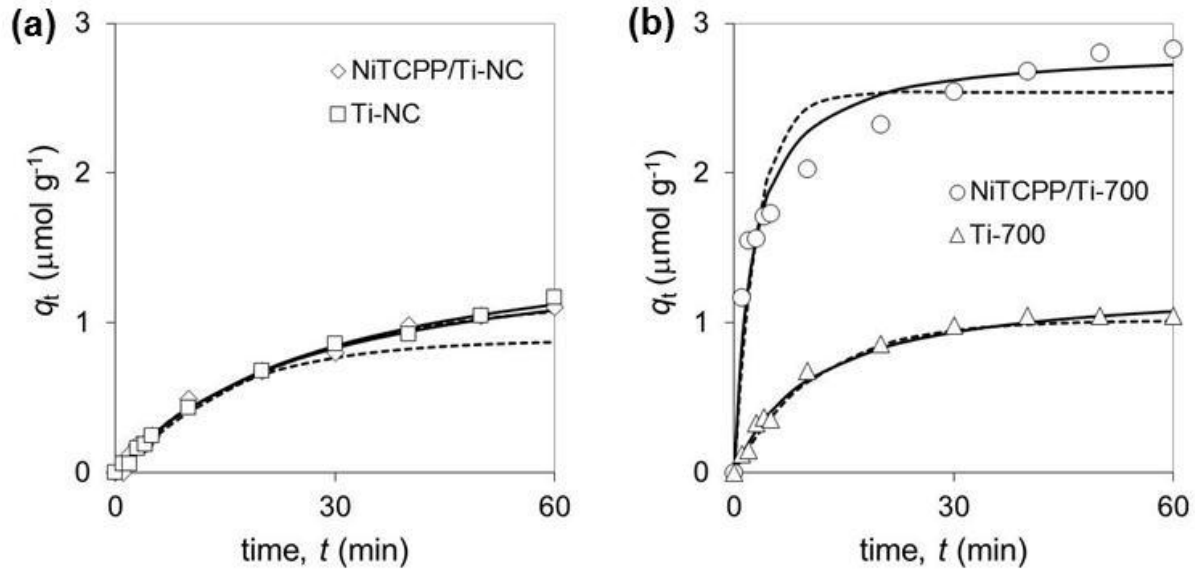

Figure 4. Evolution of MB concentration of as a function of time: 60 min in the dark followed of 120 min under visible light irradiation.

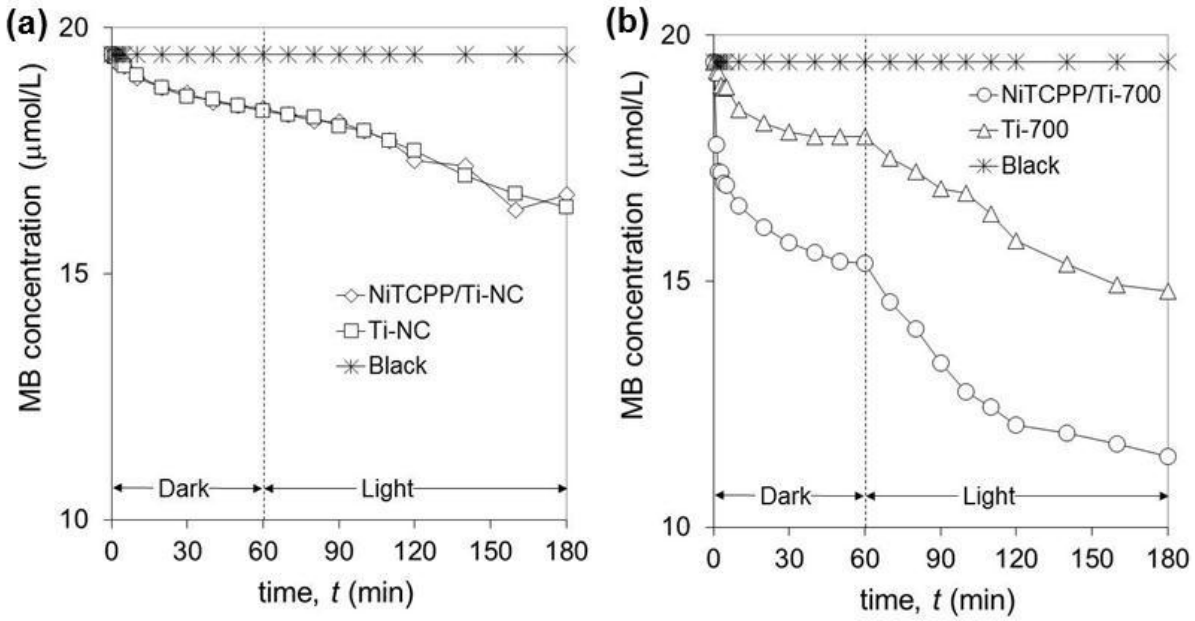

Figure 5. First-order relationship $-\ln(C/C_0) = K_{app}t$ of the MB-photoconversion under visible light irradiation.

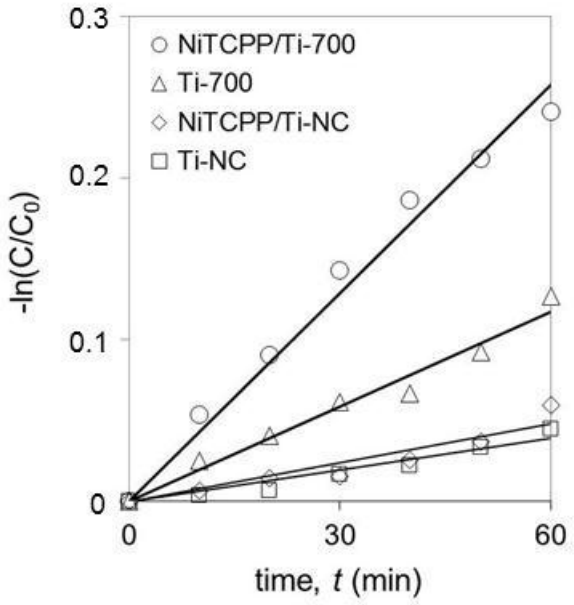

Figure 6. Schematic representation of molecular interaction between MB and porphyrin (NiTCPP) adsorbed edgewise (a) flat (b) into TiO_2-surface, and (c) their molecular structure.